Materials Science & Engineering A 685 (2017) 327–331

Contents lists available at ScienceDirect

Materials Science & Engineering A

journal homepage: www.elsevier.com/locate/msea

Three-dimensional microstructure-based micromechanical modeling for TC6 titanium alloy

Guoju Li[a,b], Ran Shi[a,b], Qunbo Fan[a,b,*], Yumeng Xia[a,b], Hongmei Zhang[a,b]

[a] School of Materials Science and Engineering, Beijing Institute of Technology, Beijing 100081, China
[b] National Key Laboratory of Science and Technology on Materials Under Shock and Impact, Beijing 100081, China

ARTICLE INFO

Keywords:
Titanium alloys
X-ray tomography
Nanoindentation
Micromechanical modeling

ABSTRACT

A new in-depth evaluation of the micromechanical response of TC6 (Ti–6Al–1.5Cr–2.5Mo–0.5Fe–0.3Si) titanium alloy subjected to uniaxial tensile loading is performed based on micromechanical modeling. This evaluation includes reconstruction of the three-dimensional annealed microstructure (annealing at 800 °C for 2 h, then air cooled) of the alloy via dual-energy micro-computed tomography. In addition, constitutive relations of the constituent phases were determined via synchrotron-based in-situ high-energy X-ray diffraction and a self-consistent model as well as nanoindentation tests combined with finite element modeling. The results revealed that the stress concentration was translated from the primary α phase to the secondary α phase, then to the β phase. Moreover, the stress generated was re-transferred to the primary α phase when the strain was increased from 0.00 to 0.05. This transfer is indicative of crack initiation in the primary α grains.

1. Introduction

The TC6 (Ti–6Al–1.5Cr–2.5Mo–0.5Fe–0.3Si) titanium alloy, one of the most commonly used α+β type titanium alloys, is extensively employed in the aerospace industry, owing to its outstanding mechanical properties [1–3]. The mechanical properties of alloys are controlled mainly by microstructural features, including the grain size, volume fraction, and spatial distribution of the constituent phases; these features may also have a significant effect on the failure behavior of alloys [4–7]. In recent years, microstructure-based micromechanical modeling [8–12] has been used to determine the correlation between the micromechanical behavior and the microstructure of dual phase steels. The results revealed that the inhomogeneous stress/strain distributions, induced by microstructural inhomogeneity, play a key role in the ductile fracture of alloys. Until now, however, the effect of microstructural features on the accommodation of stress and strain during elastic-plastic deformation in titanium alloys has scarcely been investigated. This is especially true for the TC6 titanium alloy, which contains a mixture of equiaxed primary α grains (with an average diameter of ~10 μm) and precipitated secondary α grains in the β matrix. Mechanical-property determination of constituent phases and development of the corresponding three-dimensional (3D) microstructural model are difficult, owing to this complex microstructure. To overcome these difficulties, dual-energy micro-computed tomography (DE-MicroCT) [13,14] was employed in this study to reconstruct the 3D microstructure model of the TC6 titanium alloy. This method has the unique ability to enhance the absorption contrast among constituent phases that have similar mass densities. Furthermore, the synchrotron-based in-situ high-energy X-ray diffraction (HEXRD) technique and a self-consistent model [15,16], as well as nanoindentation tests combined with finite element modeling (FEM) [17,18], were developed to determine the mechanical properties of these phases. In addition, microstructure-based micromechanical modeling for the prediction of elastic-plastic deformation and failure initiation in the TC6 titanium alloy was successfully accomplished.

2. 3D microstructural model reconstruction for the TC6 titanium alloy

The annealed microstructure of the TC6 titanium alloy was evaluated via scanning electron microscopy (SEM). As the SEM image in Fig. 1(a) shows, this microstructure consists of an α phase (dark gray) and a β phase (bright white). Enlargement of the frame-selected area reveals that the α phase is composed of an equiaxed primary α phase and a secondary α phase, which is entangled with the β phase. A DE-MicroCT SkyScan 1172 (Bruker microCT, Kontich, Belgium) was used to enhance the absorption contrast between the constituent phases. This enhancement was performed by scanning the specimen twice with different X-ray filters and applied tube voltages. Table 1 shows both sets of scanning parameters employed at a rotation step of 0.6° and a resolution of

* Corresponding author at: School of Materials Science and Engineering, Beijing Institute of Technology, Beijing 100081, China.
E-mail address: fanqunbo@bit.edu.cn (Q. Fan).

http://dx.doi.org/10.1016/j.msea.2017.01.025
Received 12 November 2016; Received in revised form 6 January 2017; Accepted 7 January 2017
Available online 08 January 2017

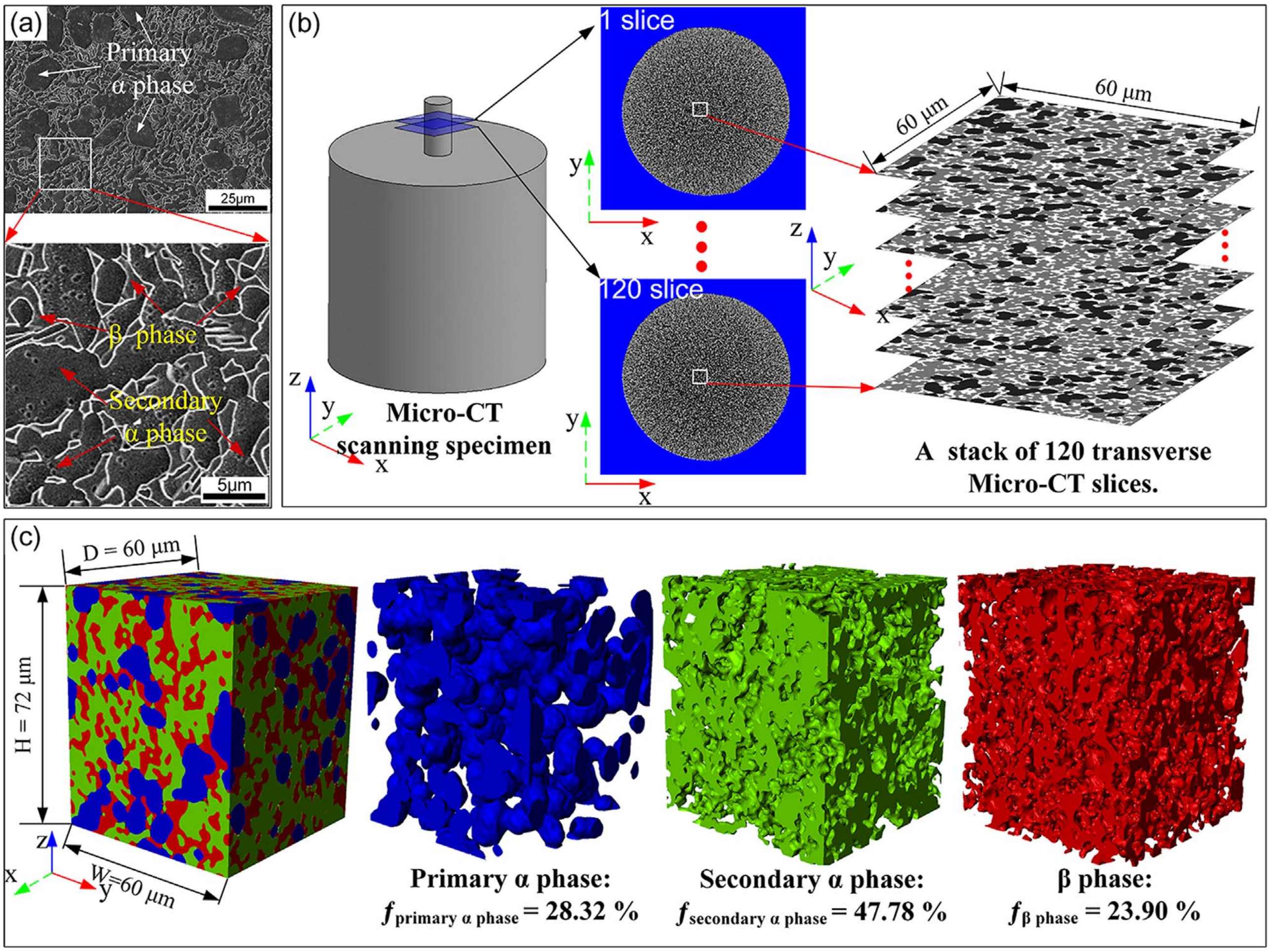

Fig. 1. 3D microstructural model reconstruction for the TC6 titanium alloy: **(a)** SEM image of annealed microstructure of the TC6 titanium alloy; **(b)** Diagram showing selection of the volume of interest in Micro-CT slices; **(c)** 3D microstructure model of the alloy.

Table 1
Dual-energy Micro-CT Scanning parameters used for the TC6 titanium alloy.

Voltage (kV)	Current (μA)	Filter	Rotation step (deg)	Resolution (μm)
59	167	0.5 mm Al	0.6	0.6
100	100	0.5 mm Al+0.5 mm Cu	0.6	0.6

0.6 μm. X-ray tube voltages of 59 kV and 100 kV and applied X-ray filters of 0.5 mm Al and 0.5 mmAl +0.5 mm Cu were used for set 1 and set 2, respectively. High-contrast low-noise micro-CT slices of the annealed microstructure were obtained after reconstruction and enhancement of the absorption contrast between each constituent phase; this enhancement was performed by using a dual-energy Micro-CT imaging program (Dehist; Bruker microCT). Details of how the absorption contrast between the constituent phases is enhanced by this imaging program were discussed in our previous work [19]. Prior to this enhancement, the volume-of-interest (VOI) of the slices (see Fig. 1(b)) was selected; 120 slices were selected in the z-axis direction (through trans-axial direction), whereas a 60 μm ×60 μm region was selected in the xy plane (frame-selected area). These slices were then imported into the Simpleware (Simpleware Ltd., Exeter, UK) software to obtain the 3D microstructure of each constituent phase of the alloy (seeing Fig. 1(c)). Volume fractions of 28.32%, 47.78%, and 23.90% were obtained for the primary α phase, secondary α phase, and β phase, respectively. Moreover, the primary α phase is composed of discrete equiaxed grains and interconnected grains; the secondary α phase interconnects with the β phase, forming a completely interconnected network.

3. Determining the constitutive relations of individual constituent phases

3.1. Determining the constitutive relations of the α and β phases

The material behavior of the constituent phases in the TC6 titanium alloy was described by the bilinear constitutive law [17], where the initial slope is the elastic modulus E, while σ_y and E_t represent the initial yield stress (defined at zero offset strain) and the tangent modulus for plastic deformation, respectively (Fig. 2(a)). The total strain ε consists of two components, namely the elastic strain, ε_e, and the plastic strain, ε_p, corresponding to the linear part of the total effective strain accumulated beyond the yield strain ε_y. The constitutive relations of the α and β phases are determined by the synchrotron-based in-situ high-energy X-ray diffraction and a self-consistent model. A schematic of the experimental set-up is shown in Fig. 2(b). In-situ synchrotron HEXRD experiments were performed in the 11-ID-C beamline at the Advanced Photon Source (APS), Argonne National Laboratory. A monochromatic X-ray beam with energy of 111 keV (and wavelength of 0.11165 Å) was used to map the lattice strain distributions of the specimen under uniaxial tensile loading. The methodology details were reported by our previous work [20]. Fig. 2(c) shows the dependence of the measured HEXRD lattice strains on the applied stress along the loading direction of the α and β phases. The stress-strain curves of each phase obtained from the self-consistent (SC) model are shown in Fig. 2(d). Bilinear constitutive law parameters (E, σ_y, E_t) of (117.9 GPa, 3.5 GPa, 920 MPa) and (103.4 GPa, 1.6 GPa, 996 MPa) were obtained for the α and β phases, respectively.

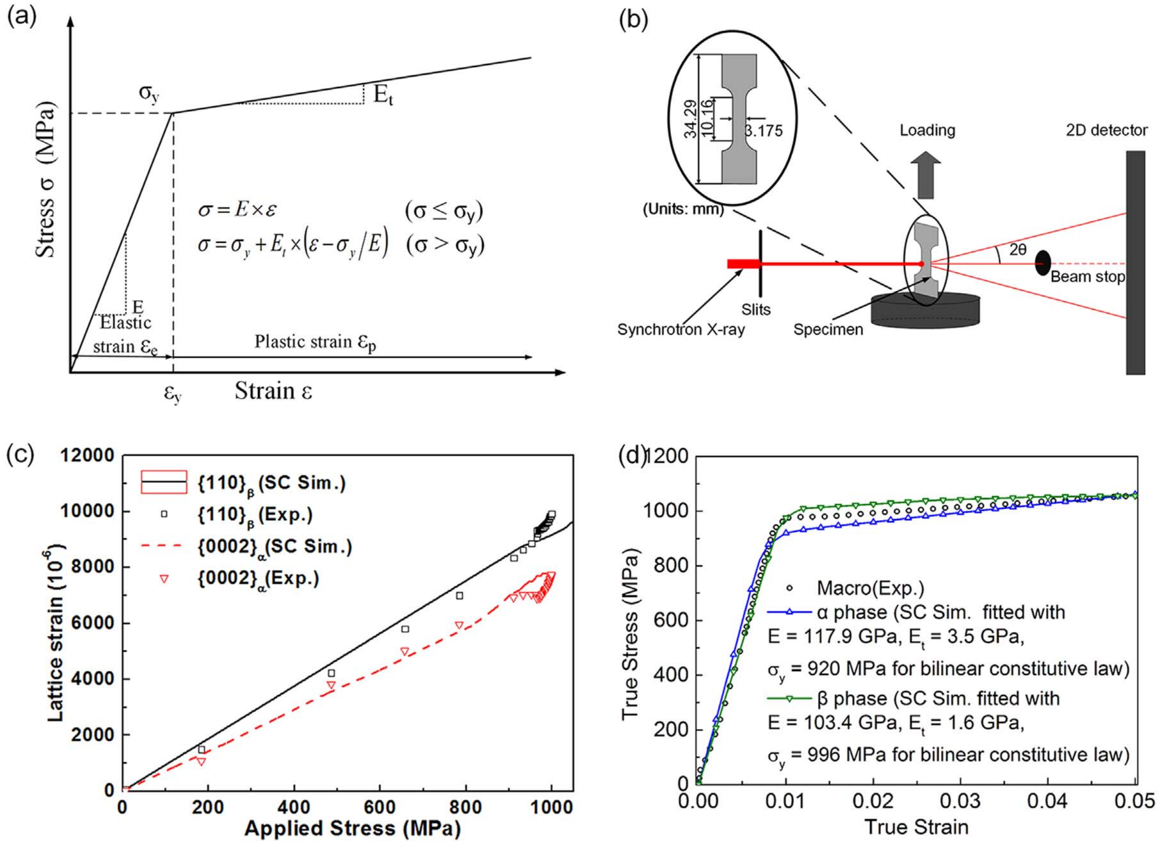

Fig. 2. Determining the constitutive relations of the α and β phases: (a) Schematic of the bilinear constitutive law; (b) Experimental set-up for in-situ loading studies performed via HEXRD; (c) Dependence of the lattice strains, measured via HEXRD, on the applied stress for different reflections along the loading direction of the α and β phases (d) Stress-strain curves of each phase, as determined via the SC model.

3.2. Determining the constitutive relations of the primary α phase

The commercial software Ansys/LS-Dyna was used to simulate the deformation process of nanoindentation (see Fig. 3(a)) of a 10×10×5 μm^3 (length×width×height) workpiece. A Berkovich indenter was used; this indenter has a triangular-based pyramid, which was modeled as an isotropic, purely elastic solid with Poisson's ratio and Young's modulus of ν_i =0.07 and E_i =1100 GPa [16], respectively. In addition, FEM was used to fit the experimental load-displacement data obtained from the nanoindentation tests on the primary α phase in the TC6 titanium alloy. The constitutive parameters were varied (E: 118–150 GPa, σ_y: 800–1000 MPa, and E_t: 3.5–10 GPa) in order to match the simulated curves with the experimental ones. After a parametric study consisting of 216 trials, we obtained a few bilinear constitutive law parameters (135 GPa, 880 MPa, 6.5 GPa), as shown in Fig. 3(b). As the figure shows, the simulation of the 500-nm-load displacement curve, as well as the shape and size of the nanoindent are well-matched with the experimental results.

3.3. Determining the constitutive relations of the secondary α phase

Based on the rule of mixtures [4,21], as expressed through Eq. (1), the bilinear constitutive law parameters (103.4 GPa, 944 MPa, 1.7 GPa) were estimated from those of the secondary α and primary α phases. The corresponding parameters for constituent phases in the TC6 titanium alloy are listed in Table 2. The results show that, in terms of mechanical properties, the secondary α phase is more similar to the β phase than to the primary α phase.

$$\sigma_\alpha(\varepsilon) = \overline{f}_{\alpha''} \times \sigma_{\alpha''}(\varepsilon) + \overline{f}_{\alpha'} \times \sigma_{\alpha'}(\varepsilon) \tag{1}$$

Where σ_α (ε), $\sigma_{\alpha'}$ (ε) and $\sigma_{\alpha''}$ (ε) are the true stresses associated with the α phase, primary α phase, and secondary α phase, respectively; $\bar{f}_{\alpha'}$ (37.2%) and $\bar{f}_{\alpha''}$ (62.8%) are the corresponding proportions in α phase.

4. Finite element analysis based on a 3D microstructure model of TC6 titanium alloy subjected to uniaxial tension loading

Numerical simulations are performed by using an Ansys/LS-Dyna code to model the micromechanical response of TC6 titanium alloy subjected to uniaxial tensile loading at a constant strain rate of $1.0\times10^{-5}s^{-1}$ (see Fig. 4(a)). An upward displacement was imposed on the top of the model, whereas the bottom was fixed. The macroscopic engineering stress is defined by dividing the reaction force (summed over the top nodes) by the initial area of the top. Similarly, the macroscopic engineering strain is obtained by dividing the z-direction displacement of the top nodes by the initial length of the model in the z direction (H_0). The true stress-strain curve is obtained from the engineering stress-strain curve, in accordance with Eqs. (2) and (3).

$$\varepsilon_t = \ln(1+\varepsilon) \tag{2}$$

$$\sigma_t = (1+\varepsilon)\sigma \tag{3}$$

where ε and σ are the macroscopic engineering strain and macroscopic engineering stress, respectively.

The simulated true stress-strain response (Fig. 4(b)) concurs with the experimentally determined response, which illustrates the current model just considering isotropic bilinear constitutive law is acceptable. The entire elastic plastic deformation process can be divided into four stages, based on the stress concentration among the constituent phases in the alloy. These stages are the: (I) first stress concentration (ε_t

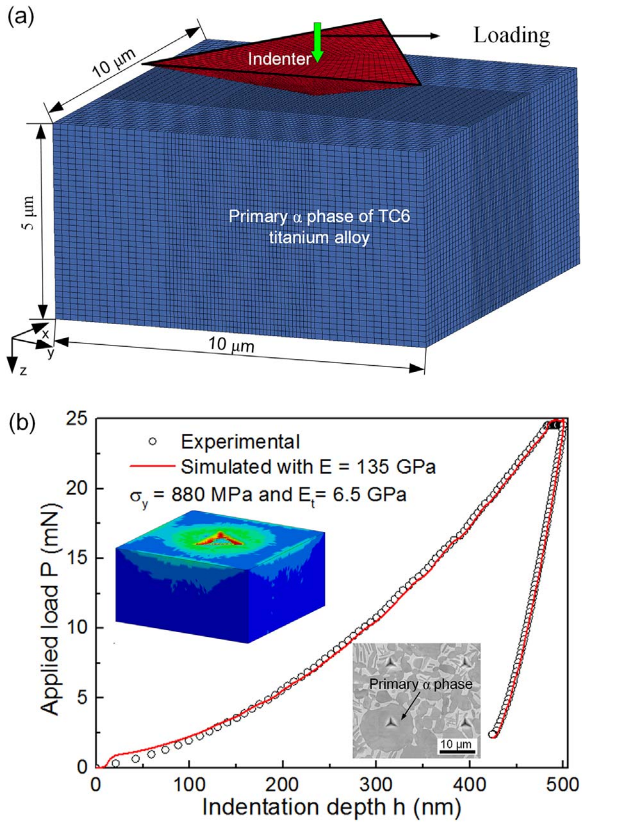

Fig. 3. Determining the constitutive relations of the primary α phase: (a) 3D nanoindentation model setup and (b) comparison of numerical and experimental P-h curves as well as the shape and size of the nanoindent in the primary α phase of the TC6 titanium alloy.

Table 2
Bilinear constitutive law parameters for constituent phases in the TC6 titanium alloy.

Constituent phases of the TC6 titanium alloy	Elastic modulus E (GPa)	Yield stress σ_y (MPa)	Tangent modulus E_t (GPa)
Primary α phase	135	880	6.5
Secondary α phase	108.9	944	1.7
β phase	103.4	996	1.6

$\le$0.007) in the primary α phase, (II) stress concentration in the secondary α phase (0.007 < ε_t $\le$0.009), (III) stress concentration in the β phase (0.009$\le\varepsilon_t$ $\le$0.010), and (IV) second stress concentration in the primary α phase (0.010 < ε_t $\le$0.05). The effective stress contours at A, B, C, and D, as shown in Fig. 4(b), are used in the analysis of these stages. Compared to the secondary α phase, the primary α phase has a lower yield stress and higher Young's modulus, and therefore experiences a stress concentration first (at point A; ε_t =0.007). Plastic deformation of the primary phase begins at this point. However, plastic deformation of the secondary α phase starts at a higher stress concentration (ε_t =0.009 vs. ε_t =0.007), i.e., at point B. This indicates that once the primary phase yields and deforms plastically, more stress is borne by the secondary phase, when ε_t increases from 0.007 to 0.009. Similarly, the stress concentration occurs mainly in the β phase at C (ε_t =0.010), where the β phase starts to deform plastically. This indicates that the stress concentration is released by plastic deformation of the primary and secondary α phases, and is transferred to the β phase when ε_t increases from 0.007 to 0.009. Interestingly, at point D (ε_t =0.050), the stress concentration is re-distributed in the primary α phase, which has a significantly higher tangent modulus (for plastic deformation) than the other constituent phases. Therefore, when ε_t increases from 0.009 to 0.050, the stress concentration is gradually transferred from the β phase to the primary α phase, thereby rendering crack nucleation at the primary α grains more favorable.

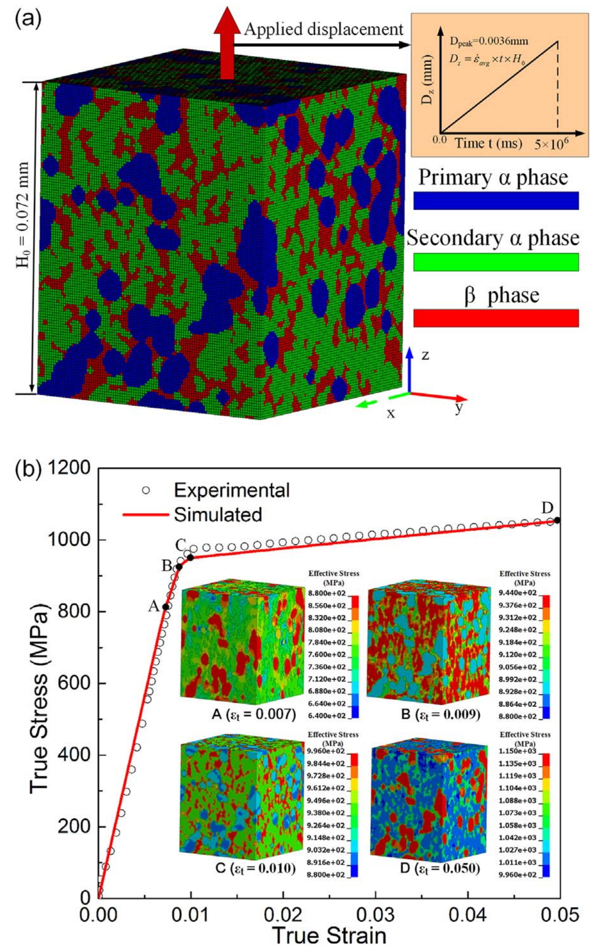

Fig. 4. Finite element analysis based on a 3D microstructure model of TC6 titanium alloy subjected to uniaxial tension loading: (a) 3D microstructure finite element model of the TC6 titanium alloy; (b) Numerical and experimental true stress-strain responses obtained under tensile loading, and effective stress contours at points A (ε_t =0.007), B (ε_t =0.0088), C (ε_t =0.010), and D(ε_t =0.050).

5. Conclusions

A 3D microstructure-based micromechanical model was developed to evaluate the micromechanical response of a TC6 titanium alloy subjected to uniaxial tensile loading. The process of stress-concentration translation among the constituent phases was observed and applied to the prediction of failure initiation in the alloy. The results revealed that the stress concentration translated from the primary α phase to the secondary α phase, then to the β phase, and again to the primary α phase. This re-transference is indicative of crack nucleation at the primary α grains.

Acknowledgements

We gratefully acknowledge the funding support from project 51571031 of the Chinese National Natural Science Foundation. The assistance of Application Engineer Xiao-ming Zhang (Beijing ZKBC Testing and Technology Co., Ltd.) with nanoindentation testing is greatly appreciated.

References

[1] E. Ghasemi, A. Zarei-Hanzaki, S. Moemeni, M. Ghambari, M. Rezaee, Mater. Sci. Eng.: A 654 (2016) 264–270.
[2] C. Pei, Q. Fan, H. Cai, J. Li, J. Alloy. Compd. 489 (2010) 401–407.
[3] M. Li, A. Xiong, W. Huang, H. Wang, S. Su, L. Shen, Mater. Charact. 49 (2002) 203–209.
[4] S. Katani, F. Madadi, M. Atapour, S. Ziaei Rad, Mater. Des. 49 (2013) 1016–1021.
[5] K.S. Choi, W.N. Liu, X. Sun, M.A. Khaleel, Acta Mater. 57 (2009) 2592–2604.
[6] X. Sun, K.S. Choi, W.N. Liu, M.A. Khaleel, Int. J. Plast. 25 (2009) 1888–1909.
[7] R. Shi, Z. Nie, Q. Fan, G. Li, J. Alloy. Compd. 688 (2016) 787–795.
[8] S.K. Paul, Mater. Des. 44 (2013) 397–406.
[9] S.K. Paul, A. Kumar, Comput. Mater. Sci. 63 (2012) 66–74.
[10] S. Sodjit, V. Uthaisangsuk, Mater. Des. 41 (2012) 370–379.
[11] M. Ohata, M. Suzuki, A. Ui, F. Minami, Eng. Fract. Mech. 77 (2010) 277–284.
[12] S.K. Paul, Comput. Mater. Sci. 56 (2012) 34–42.
[13] L.A.Fitri, V.Asyana, T.Ridwan, F.Anwary, H.Soekersi, F.D.E.Latief, F.Haryanto, J. Phys.: Conf. Ser., 694 012053, 2016.
[14] J. Paul, R.W. Bauer, W. Maentele, T.J. Vogl, Eur. J. Radiol. 80 (2011) 612–619.
[15] N. Jia, Z. Cong, X. Sun, S. Cheng, Z. Nie, Y. Ren, P. Liaw, Y. Wang, Acta Mater. 57 (2009) 3965–3977.
[16] M.R. Daymond, C.N. Tomé, M.A.M. Bourke, Acta Mater. 48 (2000) 553–564.
[17] H. Pelletier, Tribology Int. 39 (2006) 593–606.
[18] K.D. Bouzakis, N. Michailidis, Mater. Charact. 56 (2006) 147–157.
[19] G. Li, R. Shi, Q. Fan, Y. Xia, H. Zhang, Mater. Sci. Eng.: A 675 (2016) 212–220.
[20] R. Shi, G. Li, Z. Nie, Q. Fan, Mater. Sci. Eng.: A 675 (2016) 138–146.
[21] K. Chan, Y.-D. Lee, Metall. Mater. Trans. A 39 (2008) 1665–1675.